

Optical Signal Transmission through Masked Aperture to Extend the Depth of Focus in Optical Coherence Tomography

Pawan K. Tiwari¹, K. P. S. Parmar², Suman Pandey^{3*}

1- Department of Physics, Birla Institute of Technology Mesra, Ranchi, India.

Email: pawan.ktiwari@gmail.com

2-Department of Physics, University of Petroleum and Energy Studies, Dehradun, India.

Email: kpsparmar@ddn.upes.ac.in

3- Department of Computer Science and Engineering, Pohang University of Science and Technology, Pohang, South Korea.

Email: suman17july@gmail.com (Corresponding author)

Received: May 2020

Revised: August 2020

Accepted: September 2020

ABSTRACT:

Optical Coherence Tomography (OCT) imaging technique has emerged as a non- or minimally invasive modality in the clinical pathogenesis such as deep tissue examining and optical biopsy etc. The OCT imaging increases the Depth of Focus (DoF) by devising mechanisms to increase an Optical Transfer Function (OTF) of the imaging system. This is achieved through an apodization technique on the surface of lens in conjugation with the femtosecond Bessel-type laser beam. An investigation on postulation of OTF through a masked aperture, or specifically a micro-dot is investigated to measure variations of intensity profile at the optical coordinates in the radial as well as axial directions. The intensity variations in the radial and axial coordinates are calibrated to obtain the information, which significantly helps in devising of OCT imaging system. A theoretical investigation of OTF matching the experimental relationship between spot size and DoF in response to obscuration ratio is presented in this paper. This mathematical approach could be applied to different types of masking functions by meticulously exploring the parameters of optical coordinates.

KEYWORDS: Optical Transfer Function, Geometrical Coordinate, Optical Coordinate, Spot Size, Depth of Focus, Obscuration, Pupil Function.

1. INTRODUCTION

The advancement in an Optical Coherence Tomography (OCT) imaging technique has revolutionized the cell biopsy in accurate diagnosis of the disease and its treatment during pre- and post-surgical procedures [1]. It is preferred over the common stained histological examination due to one of the robust reasons that an OCT imaging is a real-time non- or minimally invasive diagnostic technique involving minimal sampling errors [2]. Moreover, due to its high resolution, such OCT has numerous applications in the area of retinal imaging in ophthalmology [3-4], brain tissue imaging [5], and deep tissue imaging [6-7], etc. The high resolution of OCT is achieved via increasing the depth of focus (DoF) of an optical beam and via minimizing an attenuation of backscattered light from the tissues by selecting the wavelength of the order of ca. ~1300 nm [7]-[8]. The common endoscopic type of OCT imaging system such as Stratus OCT is composed of swept laser source (probe beam), single-mode optical fiber, Gradient Index (GRIN) lens, and small prism to deflect focused light onto a tissue [4],[6].

The imaging system relies on studying an optical probe beam of two important factors such as its spot size and the depth of focus (DoF) [9]-[10]. The spot size of the focusing lens is given by $\lambda/(2NA)$, where λ is the wavelength and NA is the numerical aperture of that optical system. Another definitions uses the Full Width at Half Maximum (FWHM) and $(1/e^2)$ times the maximum of transmitted intensity at the focal plane of the optical system. The estimation of DoF is approximately proportional to the product of the wavelength λ and the square of the f-number (the ratio between the focal length f , and the diameter D , of the imaging lens), i.e., $\lambda(f/D)^2$. In terms of intensity, the DoF is the distance between the focal point and the point where the intensity decreases to 90%, while in application like imaging systems, it is 50% [11].

The deep tissue imaging could be achieved by increasing the DoF by using numerous types of the aperture of the imaging lens such as axicon [12], diffractive axicon [13], annular aperture [14], binary phase array of annuli [15], and cubic phase mask [16],

etc., however, limiting the resolution of the imaging system [10]. The resolution could be overcome by utilizing the non-diffracting beams such as Bessel beam [17] or Airy beam [18] with patterned aperture through the process of lithography [19-20]. The combination of Binary Phase Masks (BPM) such as Axicon (AXI), Defocus (DF) and Spherical Aberration (SA), namely BPM of Defocus+Axicon (BPM-DF-AXI) and BPM of Defocus+Spherical Aberration (BPM-DF-SA) have significantly extended the DoF multiple fold in the domain of OCT [21].

In this article, we formulate the OTF of a masked aperture having obscuration in the center of the clear aperture. The definitions of spot size and DoF are applied for masking functions with circular obscuration, which is a kind of filter with a quadratic radial transmittance [22]. The section 2 delve into the analytical analysis of OTF of an obscured mask, also referred as pupil function. Results are discussed in the section 3, and the concluding remarks are made in the section 4.

2. ANALYTICAL APPROACH

An understanding of the coordinates system and extended Depth of Focus (E-DoF) is essential in the examining the Optical Transfer Function (OTF) to investigate the spot size and DoF of the imaging system. The coordinate systems encompass geometrical and optical coordinate systems, the former one refers to point at the center of the lens on the principle axis, whereas the latter one refers to the focal point on the principle axis. The radial (r) and axial (z) geometrical distances are transformed into the radial (v) and axial (u) optical normalized coordinates which are utilized in estimating the spot size and DoF. It must be remembered that at the focal point, $r = z = 0 = v = u$. The schematic of the masked aperture, coordinate systems and E-DoF is shown in Fig. 1.

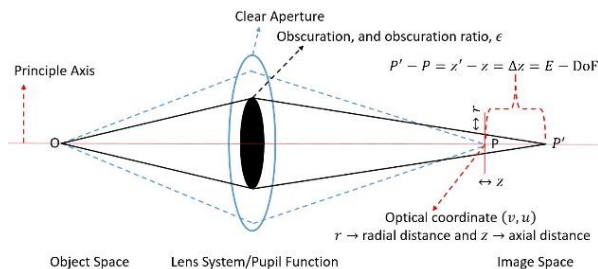


Fig. 1. Schematic of Obscuration, Optical Coordinate and Depth of Focus (DoF).

The masking of the aperture extends the intensity from point P to P' (cf. Fig.1), and the Depth of Focus (DoF), Δz is measured by analyzing axial optical coordinate u in the amplitude equation $U(v, u)$ of the Optical Transfer Function (OTF). On the other hand, spot size is calculated by analyzing v in the amplitude

equation. The masking of aperture or obscuration introduces a mathematical function, say $M(m)$ in the amplitude equation, otherwise it is unit when an aperture is clear one. The Optical Transfer Function (OTF) in the radial (v) and axial (u) optical coordinates for a masking function $M(m)$, where m is a normalized pupil, radius is written as [22]-[25],

$$U(v, u) = \frac{2}{(1-\epsilon^2)} \int_0^1 M(m) J_0(v m) \exp(i u m^2/2) m dm \quad (1)$$

Where, J_0 corresponds to zero order Bessel function of the first type, and ϵ is the central obscuration ratio.

The expression for the radial and optical coordinates can be expressed as,

$$v = k r \sin \alpha \quad (2)$$

$$u = 4 k z \sin^2(\alpha/2) \quad (3)$$

Where, $k = 2\pi/\lambda$, $\sin \alpha$ is numerical aperture,

Eq. (1) can be disintegrated further to estimate the spot size and DoF by eliminating u and v in the optical planes, respectively. The mathematical integral for the spot size and DoF can be expressed by Eq. (4) and Eq. (5), respectively

$$U(v, 0) = \frac{2}{(1-\epsilon^2)} \int_0^1 M(m) J_0(v m) m dm \quad (4)$$

$$U(0, u) = \frac{2}{(1-\epsilon^2)} \int_0^1 M(m) \exp(i u m^2/2) m dm \quad (5)$$

It should be noted that the expression $U(v, 0)$ and $U(0, u)$ gives the identical amplitude of the OTF values at the Focal Point, P . The square of the amplitude equation, $U(v, u)$ gives the intensity transmitted through the obscured aperture, which are then calibrated to estimate the spot size and depth of focus.

3. RESULTS AND DISCUSSION

The mathematical function of the various pupil functions such as Axicon (AXI), Defocus (DF), and Spherical Aberration (SA) are studied to be $M_{AXI}(m) = \exp(-2\pi i \alpha m)$, $M(m) = \exp(-2\pi i \psi m^2)$, and $M_{SA}(m) = \exp(-2\pi i \gamma m^4)$, respectively; where α , ψ , and γ refers to the slope coefficient of the axicon, defocus parameter, and strength of the spherical aberration, respectively. The pupil functions AXI, DF, and SA are combined as DF-AXI, and DF-SA as [21]

$$M_{DF-AXI}(m) = \exp(-2\pi i (\psi m^2 + \alpha m)), \quad (6)$$

and

$$M_{DF-AXI} = \exp(-2\pi i (\psi m^2 + \gamma m^4)), \quad (7)$$

Respectively, the intensities are investigated by adjusting the values of α , ψ , and γ . The DoF is measured by estimating the Strehl ratio (S) which is also referred to as DoF gain (G_{DoF}), defined as the ratio of DoFs of combined pupil function with respect to the clear aperture. The DoF gains for the pupil functions expressed by Eq. (6) and Eq. (7) which were, 5.04 and 5.03, respectively. While the Strehl ratio (S) for the pupil functions expressed by Eq. (6) and Eq. (7) were $\sim 19.5\%$ and $\sim 15.6\%$, respectively. The increase in the Strehl ratio (S) is an indication of the increase in the DoF

We focus on the result of the pupil function created through the laser micro-marking technique which is shown in Fig.1, and the masking function for the clear and masked apertures are considered as $M(m) = 1$ and $M(m) = (m^2)^n$, respectively [22]. It should be noted that the n could be integer and rational numbers. For example, $M(m)$ could be functions of types m^2 , $(m^2)^{1/n}$, $(2m^2 - 1)^{2/n}$, etc. [22]. Utilizing the masking expression $M(m) = m^2$ in Eq. (1), the intensity variation at the focal plane for the various obscuration ratio is shown in the Fig.2.

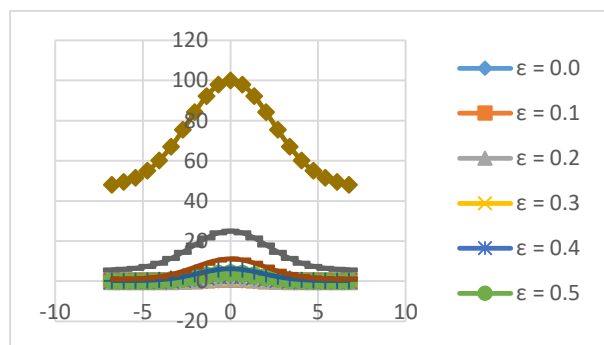


Fig. 2. Intensity variation at the focal plane with respect to obscuration ratio.

It is observed that with the increasing obscuration ratio, the intensity increases at the focal plane. The spot size is related to the distance between the extremes of the curve in Fig. 2 where the intensity drops to $1/e^2$ times the maximum intensity, upon calibration of Eq. (4), the spot size was observed to be of the order of μm . Similarly, utilizing the concept of variation of the intensity of the optical beam in the axial direction where the intensity drops by 50% of the maximum intensity, depth of focus calibrated using Eq. (5) was observed to be of the order of mm . The plot of variation of spot size and depth of focus with varying obscuration ratio is shown in Fig. 3.

The parameters used to solve the amplitude equation (Eq. 1) are $D = 120 \mu m$, $\lambda = 1.3 \mu m$ and numerical aperture, $\sin\alpha = 0.14$. The experiments that were conducted to obtain the simulation parameters are described briefly to corroborate the parameters. The different diameter micro-dots were marked on the

surface of the glass tube induced by a femtosecond laser (Pharos, Light conversion) with pulse duration of 230 fs and a pulse peak power of 4.3 MW using a $20\times$ objective lens with a focal length of 10 mm, a spot diameter of 3 μm , and a DoF of 1.7 μm . The high peak intensities with femtosecond pulses activated micro-processing of miniature transparent modules with a high precision. The obscuration was defined as the ratio of the micro-dot area and the beam propagation area of the glass tube which is perpendicular to the optical axis. A $5\times$ objective lens (LSM03, Thorlabs) with an effective focal length of 36 mm was used to magnify the OTF. To measure the axial and radial OTFs, a light source (BM-100-SCA-1310-9/125-S, OZ optics) centered at 1310 nm with a bandwidth of 40 nm and the beam profiler (BP209-IR/M, Thorlabs) were utilized. Optical simulation using ZEMAX software (ZEMAX Development Corp., WA, USA) was also performed to compare theoretical and experimental values.

For a clear aperture, a spot diameter and a DoF were 38.5 μm and 1.25 mm, respectively. However, with the increase in the obscuration ratio (ϵ), a DoF enhanced, but a spot diameter slightly decreased. The DoF was enhanced by 2.2 mm at $\epsilon = 0.7$ with a spot diameter of 33 μm . This analysis could propel devising a low cost OCT device to fabricate and implement in the clinical investigations commercializing the E-DoF optical probes

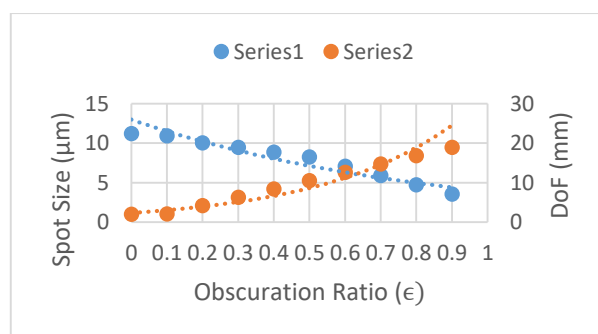


Fig. 3. Spot Size at the focal plane with respect to obscuration ratio.

4. CONCLUSION

The motivation of this communication was to find a correlation between the variation of spot size and depth of focus in the optical coordinates with respect to the obscuration ratio for the micro-dot pupil function which were not well documented in the research journals. The complete understanding of v , u and $M(m)$, and subsequently the mathematical verification of experimental variation of spot size and DoF with respect to the obscuration ratio might entail an exhaustive analysis of masking functions incorporated in the *Optics Express* research article. The understanding of amplitude equation and masking functions would be

significantly helpful in designing the probe of an imaging system comprising of a combination of elements such as graded-index fiber, no-core fiber, dispersion-shifted fiber etc. The imaging elements may be considered lumped into a single black box, and the significant properties of the system can be completely described by specifying only the terminal properties of an aggregate, that is, entrance and exit pupils. The optical transfer function of an entrance pupil could be *Circular Function*, while the masking function of the exit pupils could be *Quadratic and Exponential* for circular and ring type obscurations, respectively.

5. ACKNOWLEDGMENT

The authors gratefully acknowledge Prof. Jinyong Ha, Department of Electrical Engineering, Sejong University, South Korea for providing his laboratory facilities on the original version of this article.

REFERENCES

- [1] J. T. Yap, J. P.J. Carney, N.C. Hall, D. W. Townsend, "Image-guided cancer therapy using PET/CT," *Cancer J.*, Vol. 10, pp. 221-33, Jul. 2004.
- [2] D. Huang, E. A. Swanson, C. P. Lin, J. S. Schuman, W. G. Stinson, W. Chang, M. R. Hee, T. Flotte, K. Gregory, C. A. Puliafito, "Optical coherence tomography", *Science*, Vol. 254, pp. 1178-1181, Nov. 1991
- [3] E. Beaurepaire, A. C. Boccara, M. Lebec, L. Blanchot, and H. S. Jalmes, "Full-field optical coherence microscopy," *Opt. Lett.*, Vol. 23, pp. 244-246, Feb. 1998.
- [4] M. Adhi, J. S. Jucker, "Optical coherence tomography-current and future applications," *Cur. Opin. Ophthalmol.*, Vol. 24, pp. 213-221, May 2013.
- [5] O. Assayag, K. Grieve, B. Devaux, F. Harms, J. Pallud, F. Chretien, C. Boccara, P. Varlet, "Imaging of tumorous and non-tumorous human brain tissues with full-field optical coherence tomography," *NeuroImage Clin.*, Vol. 2, pp. 549-557, Feb. 2013.
- [6] W. Jung, S. A. Boppart, "Optical coherence tomography for rapid tissue screening and directed histological sectioning," *Anal. Cell Pathol. (Amst.)*, Vol. 35, pp. 129-143, Jan. 2012.
- [7] Y. Zhao, W. J. Eldridge, J. R. Maher, S. Kim, M. Crose, M. Ibrahim, H. Levinson, A. Wax, "Dual-axis optical coherence tomography for deep tissue imaging," *Opt. Lett.*, Vol. 42, pp. 2302-2305, Jun 2017.
- [8] B.Unterhuber, B. Povazay, H. Hermann, "In vivo retinal optical coherence tomography at 1040 nm-enhanced penetration into the choroid," *Opt. Express.*, Vol. 13, pp. 3252-3258, May 2005.
- [9] H. Wang, G. Yuan, W. Tan, L. Shi, T. Chong, "Spot size and depth of focus in optical data storage system," *Opt. Eng.*, Vol. 46, pp. 065201-1~3, Jun. 2007.
- [10] Z. Zalevsky, "Extended depth of focus imaging: A review," *SPIE Rev.*, Vol. 1, pp. 018001-1~11, Jan. 2010.
- [11] C. J. R. Sheppard, "Depth of field in optical microscopy," *J. Microsc.*, Vol. 149, pp. 73-75, Oct. 1987.
- [12] J. H. Mcleod, "The axicon: A new type of optical element," *J. Opt. Soc. Am.*, Vol. 44, pp. 592-597, Aug. 1954.
- [13] J. Dyson, "Circular and spiral diffraction gratings," *Proc.R. Soc.Lond A Math. Phys. Sci.*, Vol. 248, pp. 93-106, Oct. 1958.
- [14] E. H. Linfoot, E. Wolf, "Diffraction images in systems with an annular aperture," *Proc. Phys. Soc. B*, Vol. 66, pp. 145-149, Sept. 1952.
- [15] H. F. Wang, F. Gan, "High focal depth with a pure phase-apodizer," *Appl. Opt.*, Vol. 40, pp. 5658-5662, Nov. 2001.
- [16] E. R. Dowski Jr., W. T. Cathey, "Extended depth of field through wave-front coding," *Appl. Opt.*, Vol. 34, pp. 1859-1866, April 1995.
- [17] D. McGloin, K. Dholakia, "Bessel beams: diffraction in a new light," *Contemp. Phys.*, Vol. 46, pp. 15-28, Jan. 2005.
- [18] G. A. Siviloglou, J. Broky, A. Dogariu, D. N. Christodoulides, "Observation of accelerating Airy beams," *Phys. Rev. Lett.*, Vol. 99, Nov. 2007.
- [19] P. Polynkin, M. Kolesik, J. V. Moloney, G. A. Siviloglou, D. N. Christodoulides, "Curved plasma channel generation using ultraintense Airy beams," *Science*, Vol. 324, pp. 229-232, April. 2009.
- [20] B. Y. Wei, P. Chen, W. Hu, W. Ji, L. Y. Zheng, S.-J. Ge, Y. Ming, V. Chigrinov, Y. Q. Lu, "Polarization-controllable Airy beams generated via a photoaligned director-variant liquid crystal mask," *Sci. Rep.*, Vol. 5, pp. 17484-1~8, Dec. 2015.
- [21] S. Ryu, C. Joo, "Design of binary phase filters for depth-of-focus extension via binarization of axisymmetric aberrations," *Opt. Express*, Vol. 25, pp. 30312-30326, Nov. 2017.
- [22] C. J. R. Sheppard, Z. S. Hegedus, "Axial behavior of pupil-plane filters", *J. Opt. Soc. Am. A*, Vol. 5, pp. 643-647, Dec. 1987.
- [23] C. J.R. Sheppard, Shalin Mehta, "Three-level filter for increased depth of focus and Bessel beam generation," *Opt. Express*, Vol. 20, pp. 27212-27221, Nov. 2012
- [24] H. F. A. Tschunko, "Imaging performance of annular aperture," *Appl. Opt.*, Vol. 13, pp. 1820-1853, Aug. 1974.
- [25] J. E. Harvey, "Diffraction effects in grazing incidence x-ray telescope," *J. Xray Sci. Technol.*, Vol. 3, pp. 68-76, Oct. 1991.